

# Electronic structure of Kondo lattice compounds $\text{YbNi}_3\text{X}_9$ ( $X = \text{Al}, \text{Ga}$ ) studied by hard x-ray spectroscopy

Yuki Utsumi,<sup>1,\*</sup> Hitoshi Sato,<sup>2,†</sup> Shigeo Ohara,<sup>3</sup> Tetsuro Yamashita,<sup>3</sup> Kojiro Mimura,<sup>4</sup> Satoru Motonami,<sup>4</sup> Kenya Shimada,<sup>2</sup> Shigenori Ueda,<sup>5</sup> Keisuke Kobayashi,<sup>2,5</sup> Hitoshi Yamaoka,<sup>6</sup> Naohito Tsujii,<sup>7</sup> Nozomu Hiraoka,<sup>8</sup> Hirofumi Namatame,<sup>2</sup> and Masaki Taniguchi<sup>1,2</sup>

<sup>1</sup>Graduate School of Science, Hiroshima University, Higashi-Hiroshima 739-8526, Japan

<sup>2</sup>Hiroshima Synchrotron Radiation Center, Hiroshima University, Higashi-Hiroshima 739-0046, Japan

<sup>3</sup>Graduate School of Engineering, Nagoya Institute of Technology, Nagoya 466-8555, Japan

<sup>4</sup>Graduate School of Engineering, Osaka Prefecture University, Sakai 599-8531, Japan

<sup>5</sup>Synchrotron X-ray Station at SPring-8, National Institute for Materials Science, Hyogo 679-5148, Japan

<sup>6</sup>RIKEN Harima Institute, Sayo, Hyogo 679-5148, Japan

<sup>7</sup>Quantum Beam Unit, National Institute for Materials Science, 1-2-1 Sengen, Tsukuba 305-0047, Japan

<sup>8</sup>National Synchrotron Radiation Research Center, Hsinchu 30076, Taiwan

(Received 21 June 2012; published 11 September 2012)

We have performed hard x-ray photoemission spectroscopy (HAXPES) for Yb-based Kondo lattice compounds; an antiferromagnetic heavy-fermion system  $\text{YbNi}_3\text{Al}_9$  and a valence fluctuation system  $\text{YbNi}_3\text{Ga}_9$ . The Yb  $3d_{5/2}$  spectra of  $\text{YbNi}_3\text{Ga}_9$  showed both  $\text{Yb}^{2+}$  and  $\text{Yb}^{3+}$ -derived structures indicating strong valence fluctuation, and the intensity of  $\text{Yb}^{2+}$  ( $\text{Yb}^{3+}$ ) structures gradually increased (decreased) on cooling. The Yb  $3d_{5/2}$  spectra of  $\text{YbNi}_3\text{Al}_9$  mostly consisted of  $\text{Yb}^{3+}$ -derived structures and showed little temperature dependence. The Yb valences of  $\text{YbNi}_3\text{Ga}_9$  and  $\text{YbNi}_3\text{Al}_9$  at 22 K were evaluated to be 2.43 and 2.97, respectively. Based on the results of the Ni  $2p$  and valence-band HAXPES spectra together with soft x-ray valence-band spectra, we described that the difference of physical properties of  $\text{YbNi}_3\text{X}_9$  ( $X = \text{Al}, \text{Ga}$ ) is derived from the differences of the  $4f$ -hole level relative to the Fermi level ( $E_F$ ) and Ni  $3d$  density of states at  $E_F$ . The HAXPES results on the Yb valences were consistent with those obtained by x-ray absorption spectroscopy using the partial fluorescence yield mode and resonant x-ray emission spectroscopy at the Yb  $L_3$  edge.

DOI: [10.1103/PhysRevB.86.115114](https://doi.org/10.1103/PhysRevB.86.115114)

PACS number(s): 75.30.Mb, 71.27.+a, 79.60.-i, 71.20.Eh

## I. INTRODUCTION

The  $4f$  orbitals in rare-earth ions are almost localized inside the  $5d$  and  $6s$  valence shells. However, the tails of  $4f$  orbitals extend out of the ions and may hybridize with conduction electrons. In strongly correlated  $4f$ -electron systems, the hybridization between the  $4f$  and conduction electrons ( $c$ - $f$  hybridization) produces a wide variety of physical phenomena such as heavy-fermion behavior, magnetic transition, valence fluctuation, and unconventional superconductivity.<sup>1</sup> A large number of studies have been performed for Ce compounds because of simplicity of their  $4f^1$  electron configuration. The studies for the Yb compounds with the  $4f^1$  hole configuration ( $\text{Yb}^{3+}$ ) are limited in number because the known Yb-compounds have often shown strong hybridization with fully occupied Yb  $4f$  orbitals ( $\text{Yb}^{2+}$ ). Recently, the first Yb-based superconductor  $\beta$ - $\text{YbAlB}_4$  with  $T_C = 80$  mK was discovered.<sup>2</sup> This compound is considered to be located near a quantum critical point, showing strong valence fluctuation with the mean Yb valence of  $\text{Yb}^{2.75+}$ .<sup>3</sup> It is suggested that the strong valence fluctuation is one possible driving force of the unconventional superconductivity in  $\beta$ - $\text{YbAlB}_4$ .

Recently, Ohara *et al.* has succeeded in synthesizing single crystals of new Yb-based Kondo lattice compounds  $\text{YbNi}_3\text{X}_9$  ( $X = \text{Al}, \text{Ga}$ ) whose physical properties strongly depend on  $X$  atoms.<sup>4,5</sup>  $\text{YbNi}_3\text{Al}_9$  is an antiferromagnetic heavy-fermion system with the Néel temperature of  $T_N = 3.4$  K. The magnetic susceptibility exhibits the Curie-Weiss behavior above 80 K and an effective magnetic moment is estimated to

be  $\mu_{\text{eff}} \sim 4.37\mu_B/\text{Yb}$ , corresponding to the Yb valence close to  $3+$ . In contrast, the magnetic susceptibility of  $\text{YbNi}_3\text{Ga}_9$  shows a typical valence fluctuation behavior with the Pauli paramagnetic ground states and it reaches a broad maximum around 200 K. The Kondo temperature  $T_K$  changes from a few K to several hundred K by substituting the  $X$  atom from Al to Ga.

$\text{YbNi}_3\text{X}_9$  possesses the trigonal  $\text{ErNi}_3\text{Al}_9$ -type crystal structure with a space group of  $R\bar{3}2$ .<sup>6,7</sup> The  $\text{Ni}_3$ ,  $\text{X}_3$  and  $\text{Yb}_2\text{X}_3$  layers with a triangular lattice stack along the  $c$  axis to be close packed. The Yb ion in the  $\text{Yb}_2\text{X}_3$  layer forms a honeycomb lattice with a  $\text{X}_3$  cluster at the center. The lattice volume varies less than 1% on the substitution of  $X$  atoms of  $\text{YbNi}_3\text{X}_9$ . Furthermore, the Al and Ga ions are isovalent with their nominal valence electron configurations of  $(3s^23p^1)$  and  $(4s^24p^1)$ , respectively. In spite of the same crystal structure and similar valence electrons,  $\text{YbNi}_3\text{Al}_9$  and  $\text{YbNi}_3\text{Ga}_9$  are located at a distance in the Doniach phase diagram.<sup>8</sup> Therefore  $\text{YbNi}_3\text{X}_9$  is suitable to investigate the difference in the electronic structures between an antiferromagnetic heavy-fermion system and a valence fluctuation system. As a similar system, we may refer to  $\text{YbM}_2\text{Si}_2$  ( $M = \text{Rh}, \text{Ir}$ ),<sup>9</sup> and the other isostructural series of  $\text{YbMCu}_4$  ( $M = \text{Au}, \text{Ag}, \text{Cd}, \text{In}, \text{Mg}, \text{Tl}, \text{Zn}$ )<sup>10,11</sup> with a wide variety of physical phenomena.

In this study, we carried out hard x-ray photoemission spectroscopy (HAXPES) with  $h\nu = 5.95$  keV in order to clarify the electronic structure of  $\text{YbNi}_3\text{X}_9$ . The Yb  $3d_{5/2}$  HAXPES spectra show that the Yb valence of  $\text{YbNi}_3\text{Al}_9$  is almost trivalent, while that of  $\text{YbNi}_3\text{Ga}_9$  strongly fluctuates in

agreement with the magnetic susceptibility measurement.<sup>4,5</sup> We report the temperature-dependent Yb valences evaluated from the fitting analysis of the Yb  $3d_{5/2}$  spectra. The Yb valence of YbNi<sub>3</sub>Ga<sub>9</sub> at 300 K is  $z \sim 2.59$  and monotonically decreases to  $z \sim 2.43$  at 22 K, while that of YbNi<sub>3</sub>Al<sub>9</sub> almost stays at  $z \sim 2.97$  between 300 and 22 K. These HAXPES results are consistent with those of the x-ray absorption spectroscopy using the partial fluorescence yield mode (PFY-XAS) and resonant x-ray emission spectroscopy (RXES) at the Yb  $L_3$  edge, except that the Yb valences obtained from the PFY-XAS and RXES experiments are closer to Yb<sup>3+</sup>. We discuss the physical properties of YbNi<sub>3</sub>X<sub>9</sub> from a viewpoint of the electronic structure based on the valence-band and Ni  $2p$  HAXPES spectra and describe that the  $4f$ -hole level and amount of the Ni  $3d$  density of states (DOS) at the Fermi level ( $E_F$ ) are keys to understand their different properties of YbNi<sub>3</sub>X<sub>9</sub>.

## II. EXPERIMENTS

Single crystals of YbNi<sub>3</sub>X<sub>9</sub> were synthesized by the self-flux method as described in the literature.<sup>4,5</sup> The x-ray powder diffraction indicated the samples were in a single phase without any impurity phases. The residual resistivity of less than  $1 \mu\Omega\text{cm}$  shows high quality of the samples.<sup>4</sup>

The HAXPES experiments with  $h\nu = 5.95$  keV were performed at undulator beamline BL15XU<sup>12</sup> of SPring-8. Synchrotron radiation was monochromatized with a Si (111) double-crystal monochromator and a post Si (333) channel-cut monochromator.<sup>13</sup> The HAXPES spectra were taken by using a hemispherical analyzer (VG SCIENTA R4000) and the overall energy resolution was set to 240 meV for the Yb  $3d_{5/2}$  and valence-band spectra and 150 meV for the Ni  $2p_{3/2}$  spectra. Clean surfaces of the samples were obtained by fracturing *in situ* under the base pressure of  $1 \times 10^{-7}$  Pa at room temperature. The spectra were measured in the temperature range of 300–22 K. The binding energy of the spectra was calibrated by the Fermi edge of a gold film.

PFY-XAS and RXES measurements were performed at the Taiwan beamline BL12XU<sup>14–16</sup> of SPring-8. A Johann-type spectrometer equipped with a spherically bent Si(620) crystal

(radius of  $\sim 1$  m) was used to detect the Yb  $L\alpha_1$  ( $3d_{5/2} \rightarrow 2p_{3/2}$ ) and Raman emissions with a solid state detector (XFlash 1001 type 1201). The overall energy resolution was estimated to be about 1 eV around the emitted photon energy of 7.4 keV.

## III. RESULTS

Figure 1(a) shows the temperature dependence of the Yb  $3d_{5/2}$  HAXPES spectra of YbNi<sub>3</sub>Ga<sub>9</sub> measured between 300 and 22 K. The Yb  $3d_{5/2}$  spectral features of YbNi<sub>3</sub>Ga<sub>9</sub> is similar to that of the other Yb compounds.<sup>3,17–20</sup> The Yb<sup>2+</sup> component is observed as a prominent peak at 1520 eV, while the Yb<sup>3+</sup> components exist at 1524–1534 eV exhibiting multiplet structures arising from the Coulomb interaction between the  $3d$  and  $4f$  holes in the electron configuration of the  $3d^9 4f^{13}$  final states. A broad structure around 1543 eV is attributed to a plasmon satellite accompanied by the Yb<sup>3+</sup> $3d_{5/2}$  photoemission process.<sup>3,17</sup> The pronounced spectral intensity of the Yb<sup>2+</sup>-derived structure exhibits a clear experimental evidence of the strong valence fluctuation in YbNi<sub>3</sub>Ga<sub>9</sub>, as inferred from the temperature dependence of the magnetic susceptibility. With decreasing temperature, the intensity of the Yb<sup>2+</sup> (Yb<sup>3+</sup>) structure gradually increases (decreases), indicating that the Yb valence is closer toward Yb<sup>2+</sup> as in the other valence fluctuating compounds.<sup>3,21,22</sup>

Here, we comment on an additional structure around 1536 eV shown by a vertical bar in Fig. 1(a). This structure was not observed for YbInCu<sub>4</sub> (see Ref. 17), Yb<sub>1-x</sub>Lu<sub>x</sub>B<sub>12</sub> (see Ref. 18), and YbNi<sub>3</sub>Al<sub>9</sub> [see Fig. 2(a)], and cannot be explained by the atomic multiplet calculations. Its intensity gradually increases with decreasing temperature along with the Yb<sup>2+</sup> peak intensity, not with the Yb<sup>3+</sup>-derived spectral intensity, indicating a correlation to the Yb<sup>2+</sup> states. The structure at this energy region was reported in the Yb  $3d$  spectrum of YbAl<sub>3</sub> in Ref. 20. It was attributed to the Yb<sup>2+</sup>-derived plasmon satellite from the fact that the binding energy of the structure is higher by  $\Delta E = 15.2$  eV than that of the Yb<sup>2+</sup> peak, and it coincides well with the plasmon peak separation of  $\Delta E = 15.2$  eV in the Yb<sup>3+</sup>-derived structures. In the case of YbNi<sub>3</sub>Ga<sub>9</sub>, the structure at 1536 eV is shifted by  $\Delta E \sim 16$  eV from the

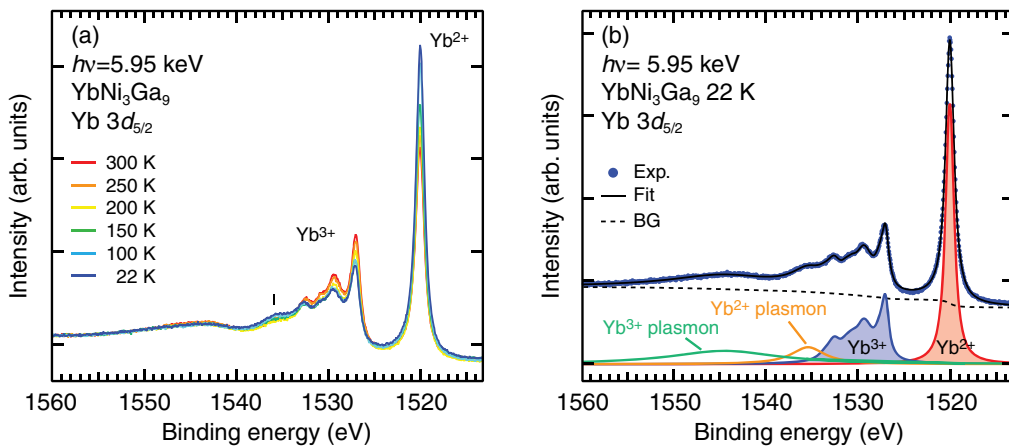


FIG. 1. (Color online) (a) Temperature dependence of the Yb  $3d_{5/2}$  HAXPES spectra of YbNi<sub>3</sub>Ga<sub>9</sub> measured from 300 to 22 K. A vertical bar shows the Yb<sup>2+</sup>-derived plasmon structure. (b) Fit of the Yb  $3d_{5/2}$  spectrum of YbNi<sub>3</sub>Ga<sub>9</sub> measured at 22 K.

$\text{Yb}^{2+}$  peak in agreement with the  $\text{Yb}^{3+}$  plasmon satellite. We believe, therefore, the additional structure is the  $\text{Yb}^{2+}$  plasmon satellite. The  $\text{Yb}^{2+}$  plasmon satellite is not clearly observed for the compounds with a small fraction of  $\text{Yb}^{2+}$ , such as  $\text{YbInCu}_4$  (see Ref. 17),  $\text{Yb}_{1-x}\text{Lu}_x\text{B}_{12}$  (see Ref. 18), and  $\text{YbNi}_3\text{Al}_9$ .

It has been pointed out that the analysis of the Yb  $3d_{5/2}$  spectrum can give Yb valence accurately in comparison with that of the Yb  $4f$  spectrum in the valence-band region.<sup>17,18</sup> We carried out the fitting analysis of the Yb  $3d_{5/2}$  spectra and evaluated the Yb valence of  $\text{YbNi}_3\text{Ga}_9$ . The Yb valence is given by  $z = 2 + I(\text{Yb}^{3+})/[I(\text{Yb}^{3+}) + I(\text{Yb}^{2+})]$ , where  $I(\text{Yb}^{3+})$  and  $I(\text{Yb}^{2+})$  denote the integrated intensities of the  $\text{Yb}^{2+}$  and  $\text{Yb}^{3+}$  components.

Figure 1(b) shows the fit of the Yb  $3d_{5/2}$  spectrum of  $\text{YbNi}_3\text{Ga}_9$  at 22 K as a typical example. We assume single line spectrum for the  $\text{Yb}^{2+}$  component and slightly modified line spectra derived from the atomic multiplet calculation for the  $\text{Yb}^{3+}$  component. The line spectra are convoluted with the Lorentzian function for lifetime broadening. In order to simulate the plasmon-derived spectral features, we assumed one Gaussian function. All components are convoluted with the Gaussian function taking into account the instrumental resolution of 240 meV. Finally, we add the background contribution derived from the secondary electrons according to the Shirley's method.<sup>23</sup> The obtained Yb valence of  $\text{YbNi}_3\text{Ga}_9$  is  $z \sim 2.43$  at 22 K in the case of Fig. 1(b).

Figure 2(a) shows the temperature dependence of the Yb  $3d_{5/2}$  HAXPES spectra of  $\text{YbNi}_3\text{Al}_9$  between 300 and 22 K. The intensity of the  $\text{Yb}^{2+}$  peak at 1520 eV is considerably weak compared to that of the  $\text{Yb}^{3+}$  structures at 1524–1534 eV, indicating that the Yb ion in  $\text{YbNi}_3\text{Al}_9$  is nearly trivalent. Almost no change with temperature is detected in the intensity of the  $\text{Yb}^{3+}$  structure. In contrast, the intensity of the  $\text{Yb}^{2+}$  peak gradually decreases and the spectral weight is shifted toward the lower binding-energy side from 300 to 150 K. The change in the  $\text{Yb}^{2+}$  spectral shape is saturated below 150 K. Note that the  $\text{Yb}^{2+}$ -derived peak of  $\text{YbNi}_3\text{Al}_9$  has anomalous spectral shape and can not be represented by a single components.

We also carried out the fitting analysis of the Yb  $3d_{5/2}$  spectra to obtain the Yb valence of  $\text{YbNi}_3\text{Al}_9$  as described

above except that no plasmon satellite was considered. The  $\text{Yb}^{2+}$  plasmon satellite is negligible because of the weak  $\text{Yb}^{2+}$  peak compared to the  $\text{Yb}^{3+}$  peak. The higher binding-energy side of the  $\text{Yb}^{3+}$  plasmon satellite (above 1540 eV) is incorporated as the background contribution. To analyze the spectral intensity of  $\text{Yb}^{2+}$  peak, we assume two components, labeled as  $P_1$  and  $P_2$  in Fig. 2(b). The intensity of the  $P_2$  component decreases with decreasing temperature from 300 to 150 K. The  $\text{Yb}^{2+}$  peak is shifted toward lower binding-energy side, and  $P_2$  intensity is almost unchanged below 150 K.

Although we cannot specify the origin of the two components for the  $\text{Yb}^{2+}$   $3d_{5/2}$  peak of  $\text{YbNi}_3\text{Al}_9$  at present, we consider it to be intrinsic to  $\text{YbNi}_3\text{Al}_9$  because its anomalous feature and temperature dependence are highly reproducible. In addition, similar spectral features are observed for the Cu substituted samples for the Ni ions of  $\text{YbNi}_3\text{Al}_9$ . Judging from their energy positions, the  $P_1$  component should correspond to the  $\text{Yb}^{2+}$  peak generally observed in Yb compounds.

For the  $P_2$  component, we first examine the surface or subsurface effects as an origin. For Yb compounds, it is known that the Yb ion in the (sub)surface region has the smaller valence than that in the bulk,<sup>19,24</sup> which may lead to a different  $\text{Yb}^{2+}$   $3d_{5/2}$  peak energy from that in the bulk regions. However, taking into account the escape depth of photoelectrons from Yb  $3d$  core with the kinetic energy of  $E_k \sim 4$  keV ( $\sim 64$  Å)<sup>25</sup> and the temperature dependence of the  $P_2$  intensity, the origin of the  $P_2$  component cannot be explained by the (sub)surface effect. Note that the  $\text{Yb}^{2+}$  peak for  $\text{YbInCu}_4$  with the relatively thick (sub)surface region can be fitted with single line spectrum.<sup>17</sup> Another possible explanation for the  $P_2$  component is that there are actually two Yb-ion sites in  $\text{YbNi}_3\text{Al}_9$ . Although the crystal structure of  $\text{YbNi}_3\text{Al}_9$  was first confirmed as  $\text{ErNi}_3\text{Al}_9$ -type structure with a single Yb site, according to the recent structure analysis by synchrotron radiation diffraction, the  $\text{Al}_3$  clusters in the  $\text{Yb}_2\text{Al}_3$  layer are partially replaced by the Yb ions yielding several Yb ion sites.<sup>26</sup> The temperature dependence of the  $P_2$  intensity, however, indicates that the disorder within the  $\text{Yb}_2\text{Al}_3$  layer decreases with decreasing temperature, which seems to be unlikely. To get further crystallographical information, the temperature-dependent x-ray diffraction experiment is in progress.

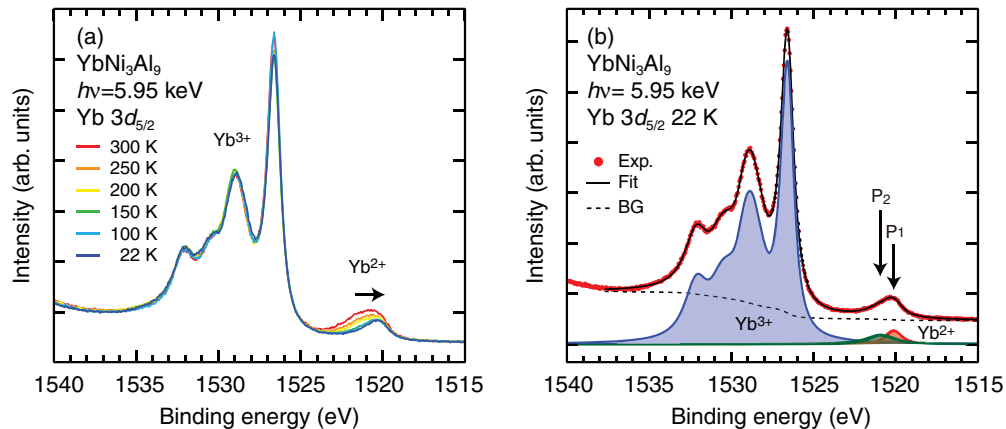


FIG. 2. (Color online) (a) Temperature dependence of the Yb  $3d_{5/2}$  HAXPES spectra of  $\text{YbNi}_3\text{Al}_9$  measured from 300 to 22 K. Spectral weight of the  $\text{Yb}^{2+}$  component is shifted toward the lower binding-energy side with decreasing temperature. (b) Fit of the Yb  $3d_{5/2}$  spectrum of  $\text{YbNi}_3\text{Al}_9$  measured at 22 K. We assume two components labeled as  $P_1$  and  $P_2$  for the  $\text{Yb}^{2+}$  peak.

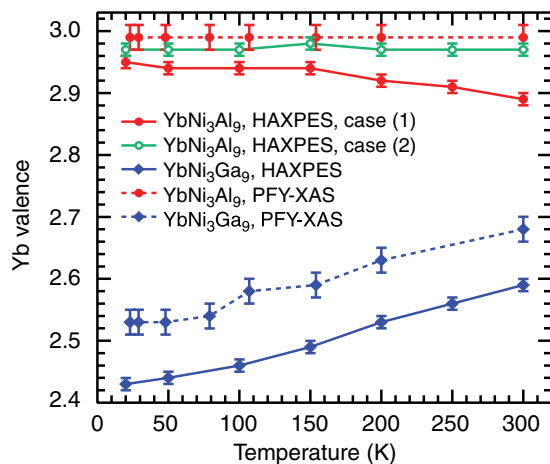


FIG. 3. (Color online) Temperature dependence of Yb valences of  $\text{YbNi}_3\text{X}_9$  ( $X = \text{Al}, \text{Ga}$ ) evaluated from the fitting analysis of Yb  $3d_{5/2}$  HAXPES and PFY-XAS spectra. Solid line connected closed and open circles represent the Yb valences from HAXPES of  $\text{YbNi}_3\text{Al}_9$  evaluated for the case (1) and case (2), respectively, while solid line connected diamonds those of  $\text{YbNi}_3\text{Ga}_9$ . Dashed line connected closed circles and diamonds represent the Yb valences of  $\text{YbNi}_3\text{Al}_9$  and  $\text{YbNi}_3\text{Ga}_9$ , respectively, from PFY-XAS.

Here, we evaluated the Yb valence of  $\text{YbNi}_3\text{Al}_9$  for the two cases: (1) we assume both  $P_1$  and  $P_2$  and (2) only  $P_1$  as the  $\text{Yb}^{2+}$  peak. In Fig. 2(b), the Yb valence at 22 K is evaluated as  $\sim 2.95$  and  $2.97$  for the cases (1) and (2), respectively.

Figure 3 shows the evaluated Yb valences of  $\text{YbNi}_3\text{X}_9$  as a function of temperature. Solid line connected closed and open circles represent the Yb valences of  $\text{YbNi}_3\text{Al}_9$  evaluated for the cases (1) and (2), respectively, while solid line connected diamonds for those of  $\text{YbNi}_3\text{Ga}_9$ . The Yb valence of  $\text{YbNi}_3\text{Ga}_9$  at 300 K is  $z \sim 2.59$  and monotonically decreases with temperature down to  $z \sim 2.43$  at 22 K. The decrease of the Yb valence is often observed for the valence fluctuation compound such as  $\text{YbAl}_3$ .<sup>21</sup> According to the single impurity Anderson model (SIAM), the Yb valence approaches toward  $\text{Yb}^{2+}$  with decreasing temperature below  $T_K$ . The present experimental results indicate that  $T_K$  of  $\text{YbNi}_3\text{Ga}_9$  is higher than room temperature, which is consistent with the temperature dependence of the magnetic susceptibility with a maximum around 200 K.<sup>4,5</sup>

The Yb valence of  $\text{YbNi}_3\text{Al}_9$  is close to  $3+$  as expected from the Curie-Weiss behavior above 80 K of the magnetic susceptibility.<sup>4,5</sup> For case (1), the evaluated Yb valence is  $z \sim 2.89$  at 300 K and gets closer to  $z \sim 3$  with decreasing temperature, which is very unusual among Yb compounds. The increase of the Yb valence at low temperature is caused by the decrease of the  $P_2$  peak. For case (2), on the other hand, the Yb valence is  $z \sim 2.97$  and shows little temperature dependence. This behavior can be explained within the framework of SIAM with low  $T_K$  less than 22 K.

To further examine the results obtained from the HAXPES measurements, we discuss PFY-XAS and RXES results at the Yb  $L_3$  edge, which are bulk-sensitive spectroscopic techniques to study the valence of Yb compounds. Figure 4(a) shows the PFY-XAS spectra of  $\text{YbNi}_3\text{Ga}_9$  taken between 300 and 23 K. The spectra were normalized to the integrated intensity. The

PFY-XAS results again indicate that  $\text{YbNi}_3\text{Ga}_9$  is the strong valence fluctuation compound. The peak at 8938 eV is derived from the  $\text{Yb}^{2+}$  component and the peak at 8945 eV is the  $\text{Yb}^{3+}$  component. The energy of the  $\text{Yb}^{3+}$  peak is higher than that of the  $\text{Yb}^{2+}$  peak because the  $\text{Yb}^{3+} 2p_{3/2}$  states with one  $4f$  hole has lower binding-energy than the  $\text{Yb}^{2+} 2p_{3/2}$  with no  $4f$  hole. With decreasing temperature, the intensity of the  $\text{Yb}^{2+}$  ( $\text{Yb}^{3+}$ ) component gradually increases (decreases). Figure 4(b) shows the RXES spectra of  $\text{YbNi}_3\text{Ga}_9$  taken at the same temperatures as the PFY-XAS spectra. The incident photon energy is set at  $h\nu = 8938$  eV, which corresponds to the  $\text{Yb}^{2+}$  peak in the PFY-XAS spectra. The horizontal axis represents an energy transfer defined as the difference between the incident and emitted photon energies. The RXES spectra mostly consist of the  $\text{Yb}^{2+}$  peak at the transfer energy of  $\Delta h\nu = 1522$  eV with a tiny broad structure around 1526–1534 eV originating from the  $\text{Yb}^{3+}$  component. It is noted that the  $\text{Yb}^{2+}$  component is emphasized in the RXES spectra excited at the  $\text{Yb}^{2+}$  peak in the PFY-XAS spectra. The temperature dependence of these components in the RXES spectra is consistent with that in the PFY-XAS spectra. Actually, the temperature dependence of the intensity ratio of  $\text{Yb}^{3+}$  to  $\text{Yb}^{2+}$  (not shown here) shows the same trend as that of the Yb valence derived from the PFY-XAS spectra.

Figures 4(c) and 4(d) exhibit the PFY-XAS and RXES spectra of  $\text{YbNi}_3\text{Al}_9$  measured with the same experimental condition for  $\text{YbNi}_3\text{Ga}_9$ . As expected from the Yb  $3d$  HAXPES spectra in Fig. 2(a), one can observe dominant  $\text{Yb}^{3+}$  component at 8945 eV in the PFY-XAS spectra and at 1528 eV in the RXES spectra. It should be noticed in the RXES spectra that the  $\text{Yb}^{2+}$  states are clearly observed as a shoulder structure at the lower transfer energy side of the  $\text{Yb}^{3+}$  peak ( $\Delta h\nu = 1522$  eV). Taking into account that the PFY-XAS and RXES are more bulk sensitive compared to HAXPES, the existence of the  $\text{Yb}^{2+}$  component in RXES spectra indicate a small fraction of the divalent Yb ions in  $\text{YbNi}_3\text{Al}_9$ . We find small peaks at 8934 eV in the PFY-XAS spectra and at 1518 eV in the RXES spectra. The similar feature is also observed in the Yb  $L_3$  PFY-XAS and RXES spectra of  $\text{YbCu}_2\text{Si}_2$  in Ref. 20, where these features are assigned to the  $2p \rightarrow 4f$  quadrupole transition.

The Yb valences of  $\text{YbNi}_3\text{X}_9$  are estimated from the fits to the PFY-XAS spectra. After the subtracting the arctan-like background from the spectra, we have fitted the spectra using the Voigt functions representing the  $\text{Yb}^{2+}$  and  $\text{Yb}^{3+}$ ,  $2p\text{-}4f$  quadrupole transition and background components shown in Fig. 5. The Yb valences are derived from the intensity ratio of the  $\text{Yb}^{2+}$  and  $\text{Yb}^{3+}$  components. The dashed lines in Fig. 3 show fitting results. The Yb valence of  $\text{YbNi}_3\text{Ga}_9$  monotonically decreases from  $z \sim 2.68$  at 300 K to  $z \sim 2.53$  at 23 K, while that of  $\text{YbNi}_3\text{Al}_9$  stays at  $z \sim 2.99$  at all temperatures. The Yb valences of  $\text{YbNi}_3\text{Al}_9$  derived from the PFY-XAS spectra are almost consistent with those of the fits of the Yb  $3d_{5/2}$  HAXPES spectra for case (1), suggesting that the analysis was appropriate. As regards  $\text{YbNi}_3\text{Ga}_9$ , the mean Yb valences deduced from the PFY-XAS spectra is about 0.15 larger than those from the Yb  $3d$  HAXPES spectra. This tendency has been widely observed for the Yb compounds. If one compares the fits in Figs. 1(b), 2(b) and 5, the analysis of the Yb  $3d_{5/2}$  HAXPES spectra is more straightforward



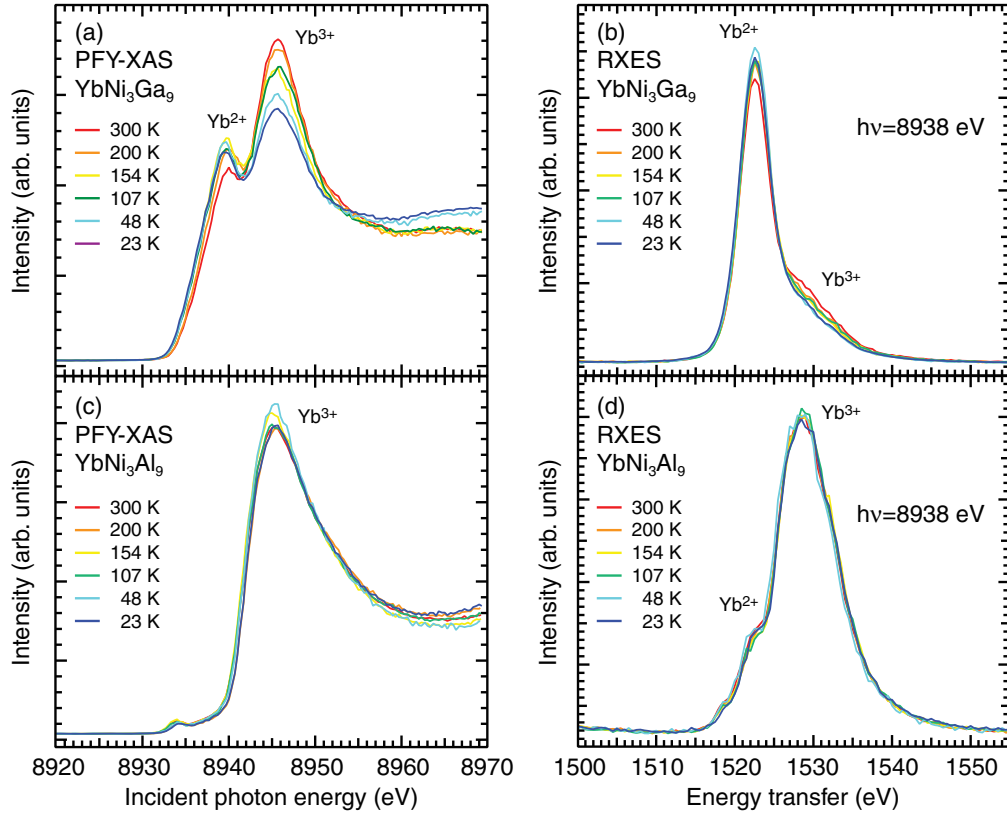


FIG. 4. (Color online) Temperature dependencies of Yb  $L_3$ -edge PFY-XAS and RXES spectra measured at 8938 eV of  $\text{YbNi}_3\text{X}_9$  between 300 and 23 K. (a) PFY-XAS and (b) RXES spectra of  $\text{YbNi}_3\text{Ga}_9$ , and (c) PFY-XAS and (d) RXES spectra of  $\text{YbNi}_3\text{Al}_9$ .

than that of the PFY-XAS spectra. In the former, the  $\text{Yb}^{2+}$  and  $\text{Yb}^{3+}$  components are separately observed, while in the latter their components are overlapped on the respective edge jumps. On the other hand, PFY-XAS is photon-in and photon-out experiments and is a more bulk sensitive compared to HAXPES using electrons as probe. Even at excitation energies as high as  $h\nu \sim 6$  keV, the HAXPES spectra might be

somewhat suffered from the surface and subsurface regions, where the Yb valence tends to be  $z \sim 2$ . This is considered to be one of the reasons why the Yb  $3d$  HAXPES provides smaller Yb valence.

Next, we examine the valence-band HAXPES spectra of  $\text{YbNi}_3\text{X}_9$ . In Fig. 6(a), the spectrum of  $\text{YbNi}_3\text{Ga}_9$  taken at 22 K exhibits the  $\text{Yb}^{2+}$  and  $\text{Yb}^{3+}$ -derived structures, indicating the valence fluctuating property. The prominent  $\text{Yb}^{2+} 4f_{7/2}$  and  $4f_{5/2}$  peaks exist near  $E_F$  and 1.5 eV, respectively, and the  $\text{Yb}^{3+} 4f$  multiplet structures due to the  $4f^{12}$  final states are observed at 5–12 eV. On the other hand, the spectrum of  $\text{YbNi}_3\text{Al}_9$  is mostly composed of the  $\text{Yb}^{3+}$  multiplet structures, consistent with the Yb  $3d_{5/2}$  spectra in Fig. 2(a). We also note the tiny peaks due to the  $\text{Yb}^{2+} 4f_{7/2}$  and  $4f_{5/2}$  states exist as shown by vertical bars. The  $\text{Yb}^{3+} 4f$  multiplet structure of  $\text{YbNi}_3\text{Al}_9$  is shifted toward the lower binding-energy side compared to that of  $\text{YbNi}_3\text{Ga}_9$  as a whole. The small peaks at 2.0 eV for  $\text{YbNi}_3\text{Ga}_9$  and at 2.3 eV for  $\text{YbNi}_3\text{Al}_9$  is ascribed to the Ni  $3d$  states. As shown in Fig. 6(b), these peaks are remarkably observed in the vacuum ultraviolet photoemission (VUVPE) spectra taken at undulator beamline BL-1 of Hiroshima Synchrotron Radiation Center (HSRC) with  $h\nu = 182$  eV, where the photoionization cross section of the Ni  $3d$  states becomes large.<sup>27</sup> Note that the Ni  $3d$  peak is shifted toward the lower binding-energy side by about 300 meV on going from  $X = \text{Al}$  to  $\text{Ga}$  as indicated by a solid line.

Figure 7 shows the Ni  $2p_{3/2}$  core HAXPES spectra of  $\text{YbNi}_3\text{X}_9$  measured at 300 K. The inset exhibits the whole Ni  $2p$  spectra in the wide binding-energy range. The Ni

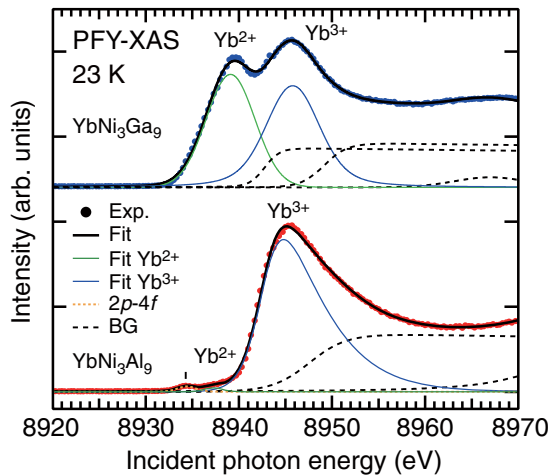


FIG. 5. (Color online) An example of the fits for PFY-XAS spectra of  $\text{YbNi}_3\text{X}_9$  at 23 K. Thin solid lines represent the fits for the  $\text{Yb}^{2+}$  and  $\text{Yb}^{3+}$  components using the Voigt functions after the subtracting the arctan-like background from the spectra.

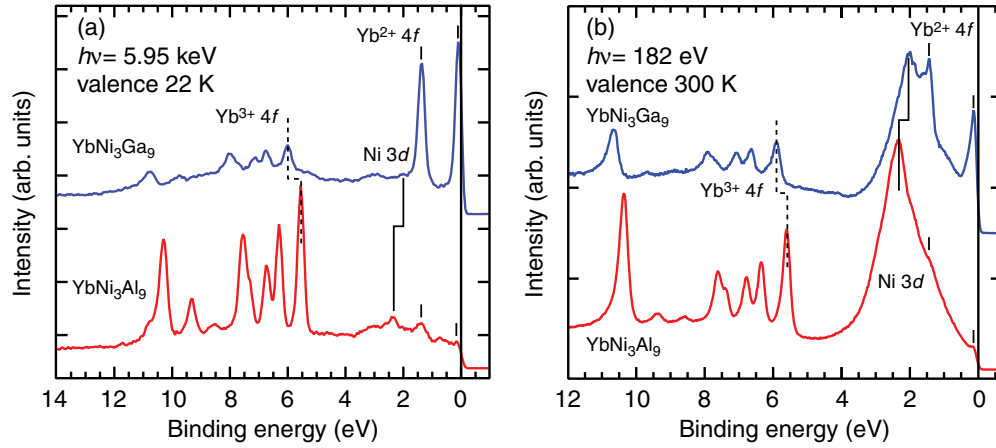


FIG. 6. (Color online) The valence-band (a) HAXPES and (b) VUVES spectra measured at 22 and 300 K, respectively. The vertical bars show the  $\text{Yb}^{2+}4f_{7/2}$  and  $4f_{5/2}$  structures. The lowest peak of the  $\text{Yb}^{3+}$  multiplet structures is shown by a dashed line. The  $\text{Yb}^{3+}4f$  multiplet structures of  $\text{YbNi}_3\text{Al}_9$  is shifted toward the lower binding-energy side compared to that of  $\text{YbNi}_3\text{Ga}_9$  as a whole. The small peaks at 2.0 and 2.3 eV in the HAXPES spectra for  $\text{YbNi}_3\text{Ga}_9$  and  $\text{YbNi}_3\text{Al}_9$  (solid line), respectively, are ascribed to the Ni 3d states, which are remarkably observed as prominent peaks in the VUVES spectra due to the large photoionization cross section of the Ni 3d states.

$2p_{3/2}$  and  $2p_{1/2}$  peaks are located around 853 and 871 eV, respectively. One can also see broad structures around 863, 880, and 887 eV, and a shoulder structure overlapping with the lower binding-energy side of the  $2p_{1/2}$  peak around 870 eV.

The bulk and surface plasmons are often observed in photoemission spectra. The energy of the surface plasmon is generally lower than that of the corresponding bulk plasmon.<sup>28</sup> The broad structure at 887 eV is ascribed to the bulk plasmon associating with the Ni  $2p_{1/2}$  photoemission and are separated from the  $2p_{1/2}$  main peak by  $\Delta E \sim 16$  eV. The Ni  $2p_{3/2}$  bulk plasmon is observed as the shoulder at 870 eV. The bulk plasmons are also observed as the broad structures at  $\Delta E \sim 16$  eV higher binding-energy from the main peaks in the Ga  $2p$  (not shown here) and Yb  $3d$  [see Fig. 1(a)] spectra

of  $\text{YbNi}_3\text{Ga}_9$ . In the inset of Fig. 7, there exist two peaks at 880 and 863 eV in the Ni  $2p$  spectra (vertical bars) that seem to be surface plasmons. However, it is unlikely because there are no corresponding peaks associating with the Ga  $2p$  spectra. Thus we consider that the structures at 880 and 863 eV are derived from the satellite structures with the  $2p^53d^9$  final states due to the electron correlation effect.<sup>29</sup>

In Fig. 7, dots and solid lines, respectively, represent the experimental spectra and the fits using the Lorentzian function convoluted with the Gaussian function for the instrumental resolution. The binding energies of the Ni  $2p_{3/2}$  states of  $\text{YbNi}_3\text{Al}_9$  and  $\text{YbNi}_3\text{Ga}_9$  are 853.80 and 853.51 eV, respectively. There exists an energy shift toward the lower binding-energy side by about 300 meV on going from  $X = \text{Al}$  to Ga. The core-level chemical shift reflects the change of the chemical bonding and charge distribution of the conduction electron around the specific atoms. Taking into account the fact that the similar energy shift is also observed for the Ni 3d states in the valence-band spectra in Fig. 6, the Ni  $2p_{3/2}$  energy shift suggests that  $E_F$  of the Ni-derived conduction-band (CB) density of states (DOS) is shifted toward the lower energy side for  $\text{YbNi}_3\text{Ga}_9$ . It suggests a charge transfer from the CB states to the Yb  $4f$  states leading to a valence fluctuation in  $\text{YbNi}_3\text{Ga}_9$ .

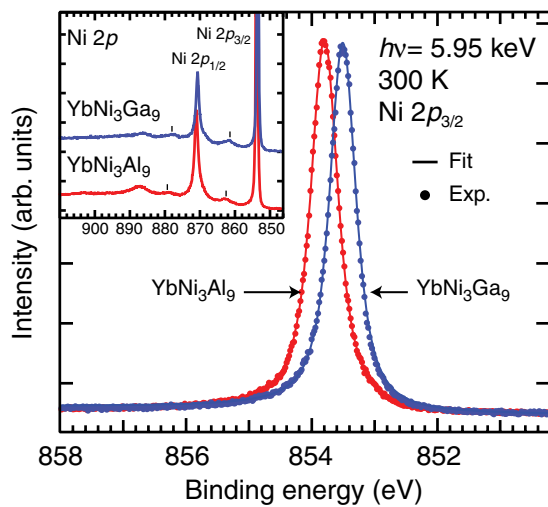


FIG. 7. (Color online) Ni  $2p_{3/2}$  HAXPES spectra of  $\text{YbNi}_3\text{Ga}_9$  and  $\text{YbNi}_3\text{Al}_9$  measured at 300 K. Dots and solid lines are, respectively, experimental spectra fits using single line spectrum convolutes with Lorentzian and Gaussian functions. The inset shows the whole region of the Ni  $2p$  spectra measured at 300 K. The broad structures shown by vertical bars are satellite structures.

#### IV. DISCUSSION

We find the difference of the binding energies of the  $\text{Yb}^{3+}4f$  multiplet structures between  $\text{YbNi}_3\text{Ga}_9$  and  $\text{YbNi}_3\text{Al}_9$  as shown by a dashed line in Fig. 6. The binding energy of the  $\text{Yb}^{3+}4f$  multiplet structures of  $\text{YbNi}_3\text{Al}_9$  are shifted by 300 meV toward the  $E_F$  side compared to that of  $\text{YbNi}_3\text{Ga}_9$ . We consider that the energy shift is originated from the difference of bare  $4f$ -hole level,  $-\epsilon_f$ , whose negative sign represents that  $4f$ -hole level exists above  $E_F$ . An energy separation of the  $\text{Yb}^{2+}$  and  $\text{Yb}^{3+}4f$  HAXPES spectra are approximately given by  $-\epsilon_f + U$ , where  $U$  stands for the Coulomb interaction between the  $4f$  holes on the same site.

If we assume that  $U$  is almost unchanged between  $\text{YbNi}_3\text{X}_9$ , the deeper binding-energy of the  $\text{Yb}^{3+}$  multiplet structures for  $\text{YbNi}_3\text{Al}_9$  suggests that the absolute value of  $-\varepsilon_f$  in  $\text{YbNi}_3\text{Al}_9$  is larger than that in  $\text{YbNi}_3\text{Ga}_9$ . This means that the  $4f$ -hole level exists far above  $E_F$  stabilizing the  $\text{Yb}^{3+}$  configuration (one hole state) in  $\text{YbNi}_3\text{Al}_9$ . On the other hand, the  $4f$ -hole level in  $\text{YbNi}_3\text{Ga}_9$  is expected to be located closer to  $E_F$  leading to the valence fluctuation.<sup>30</sup> The energy shift of the  $\text{Yb}^{3+}$  multiplet structures was also observed in  $\text{Yb}_2\text{Co}_3\text{X}_9$  ( $X = \text{Ga}, \text{Al}$ ) by VUVES with  $h\nu = 40.8$  eV.<sup>31</sup>  $\text{Yb}_2\text{Co}_3\text{Al}_9$  is an antiferromagnetic heavy-fermion compound with  $T_N = 1.16$  K and  $\text{Yb}_2\text{Co}_3\text{Ga}_9$  is a valence fluctuation compound with  $T_K \sim 210$  K as is the case of  $\text{YbNi}_3\text{X}_9$ . In addition,  $\text{Yb}_2\text{Co}_3\text{X}_9$  has similar crystal structures with that of  $\text{YbNi}_3\text{X}_9$ .<sup>32</sup>

As the  $X$  atoms are the nearest neighbor of the Yb ions, it is likely that the  $sp$ -like CB electrons derived from  $X$  atoms significantly contribute to the  $c$ - $f$  hybridization, though the band-structure calculation is yet to be performed. Furthermore, the energy shift of the Ni  $2p$  and  $3d$  states indicates that the Ni-derived CB states also contribute to the  $c$ - $f$  hybridization of  $\text{YbNi}_3\text{X}_9$ . In particular, their Ni  $3d$  DOS's should have tails toward the lower binding-energy side and some contribution to the DOS at  $E_F$  since there exist satellites in the Ni  $2p$  spectra. From the energy positions of the Ni  $3d$  peak in Fig. 6, the larger Ni  $3d$  DOS at  $E_F$  is expected for  $\text{YbNi}_3\text{Ga}_9$  compared to  $\text{YbNi}_3\text{Al}_9$ , which qualitatively explains  $T_K$  of several hundreds K for  $\text{YbNi}_3\text{Ga}_9$  and  $T_K$  of a few K for  $\text{YbNi}_3\text{Al}_9$ . In addition, based on the discussion of the energy shift of the  $\text{Yb}^{3+}4f$  multiplet structures, the Yb  $4f$ -hole level of  $\text{YbNi}_3\text{Ga}_9$  is closer to  $E_F$  than that of  $\text{YbNi}_3\text{Al}_9$ . The large Ni  $3d$  DOS and the Yb  $4f$ -hole level near  $E_F$  of  $\text{YbNi}_3\text{Ga}_9$  causes the strong hybridization between the Ni  $3d$  and Yb  $4f$  states and charge transfer from the Ni  $3d$  to Yb  $4f$  states, leading to the enhanced valence fluctuation. In the case of  $\text{YbNi}_3\text{Al}_9$ , the Yb ion stays to be trivalent because the Ni  $3d$  DOS at  $E_F$  is small and the Yb  $4f$ -hole level exists away from  $E_F$ . Thus the Ni  $3d$  DOS at  $E_F$  and the Yb  $4f$ -hole level play a key role to determine the antiferromagnetic and valence fluctuating properties of  $\text{YbNi}_3\text{X}_9$ . In order to confirm the role of the Ni  $3d$  states, studies of solid solutions of  $\text{YbNi}_3\text{X}_9$  and other transition-metal substituted systems for the Ni ions, which directly control the  $d$  band, are planned.

The Yb  $3d$  HAXPES and PFY-XAS experiments reveal that the Yb valence of  $\text{YbNi}_3\text{Ga}_9$  is close to  $z \sim 2.5$ , namely, equal population of the  $\text{Yb}^{2+}$  and  $\text{Yb}^{3+}$  states. Based on the experimental results,  $\text{YbNi}_3\text{Ga}_9$  is expected to be one of systems easy to control the magnetic ground state. In fact,  $\text{YbNi}_3\text{Ga}_9$  undergoes a transition into a ferromagnetic ordered state at  $\sim 9$  GPa.<sup>33</sup> At the critical pressure, the Yb valence is considered to be trivalent.

Generally,  $\text{Yb}^{3+}$  state is favored at high pressure indicating the decrease of  $T_K$  and the strength of  $c$ - $f$  hybridization, and the Yb ground state changes from mixed valent to localized magnetic states.<sup>34</sup> In Yb metal, the pressure induces the shift of both  $\text{Yb}^{3+}$  and  $\text{Yb}^{2+}$  energy level toward  $E_F$  and the charge transfer occurs from  $\text{Yb}^{2+}$  to CB, resulting in the enhancement of  $\text{Yb}^{3+}$ .<sup>35</sup> Our results show that the substitution of Ga to Al site in  $\text{YbNi}_3\text{Al}_9$  may correspond to apply the negative pressure and the charge transfer occurs from CB to  $\text{Yb}^{3+}$ ,

which is a reversed process of the case of Yb metal. Namely, the chemical pressure induces the charge transfer from the CB to  $4f$  hole and the localized Yb state of  $\text{YbNi}_3\text{Al}_9$  changes to the mixed valent state of  $\text{YbNi}_3\text{Ga}_9$  as described above. It is, however, noted that the difference of the lattice parameters from  $X = \text{Al}$  to  $\text{Ga}$  are about  $-0.4\%$  for  $a$  axis and  $0.8\%$  for  $c$  axis.<sup>5</sup> This indicates the difference between the chemical and hydrostatic pressure effects; in  $\text{YbNi}_3\text{X}_9$  the ground state is more sensitive to the change in the electronic structure by the chemical substitution.

Finally, we comment on the present experimental results of  $\text{YbNi}_3\text{X}_9$  in comparison with those of the valence transition compound  $\text{YbInCu}_4$ .<sup>36–38</sup> The sharp valence transition of  $\text{YbInCu}_4$  was initially observed by Yb  $L_{\alpha 1}$  resonant inelastic x-ray scattering experiments,<sup>39</sup> and then by the Yb  $3d$  HAXPES experiments.<sup>17</sup> The Yb valence derived from the HAXPES changes from  $z \sim 2.90$  to  $z \sim 2.74$  at  $T_V = 42$  K on cooling.<sup>17</sup> At  $T_V$ ,  $T_K$  also changes from  $T_{K+} \sim 25$  K to  $T_{K-} \sim 400$  K.<sup>40</sup> Recently, we found that the Cu  $2p_{3/2}$  and In  $3d_{5/2}$  peaks in the HAXPES spectra of  $\text{YbInCu}_4$  were shifted toward the lower binding-energy side below  $T_V$  by  $\sim 40$  and  $\sim 30$  meV, respectively.<sup>41</sup> The energy shifts suggest that the valence transition is caused from the charge transfer from CB to Yb  $4f$  states and the higher  $T_{K-}$  is interpreted by the higher CB-DOS at  $E_F$ . In addition, the  $\text{Yb}^{3+}4f$  multiplet structures in the valence-band soft x-ray photoemission spectra of  $\text{YbInCu}_4$  taken at  $h\nu = 800$  eV are also shifted toward the higher binding-energy side below  $T_V$ ,<sup>19</sup> again similar to the energy shift of the corresponding multiplet structures from  $\text{YbNi}_3\text{Al}_9$  to  $\text{YbNi}_3\text{Ga}_9$  (see Fig. 6). The energy shifts of the core-level and  $\text{Yb}^{3+}$  multiplet structures are, thus, possibly controlled by  $T_K$ , which may be changed through the valence transition or by the substitution of the constituent elements and pressure.

## V. CONCLUSIONS

We have investigated the electronic structure of the Kondo lattice compounds  $\text{YbNi}_3\text{X}_9$  by means of the Yb  $3d_{5/2}$ , valence-band and Ni  $2p$  HAXPES with  $h\nu = 5.95$  keV, the PFY-XAS and RXES at the Yb  $L_3$  edge, and the valence-band PES with  $h\nu = 182$  eV. Both  $\text{Yb}^{2+}$  and  $\text{Yb}^{3+}$  components were clearly observed in the Yb  $3d_{5/2}$  spectra of  $\text{YbNi}_3\text{Ga}_9$ , indicating the strong valence fluctuation, consistent with the magnetic susceptibility measurements.<sup>4,5</sup> With decreasing temperature, the intensity of the  $\text{Yb}^{2+}$  ( $\text{Yb}^{3+}$ ) structure gradually increases (decreases) and the evaluated Yb valence of  $\text{YbNi}_3\text{Ga}_9$  changes from 2.59 at 300 K to 2.43 at 22 K. The Yb  $3d_{5/2}$  spectra of  $\text{YbNi}_3\text{Al}_9$ , on the other hand, indicate that the  $\text{Yb}^{3+}$  component is dominant and the  $\text{Yb}^{2+}$  component is considerably weak. The spectra show almost no temperature dependence and the evaluated Yb valence at 22 K is 2.97, consistent with the Curie-Weiss-like magnetic susceptibility above 80 K. The results on the Yb valence and its temperature dependence were consistent with the PFY-XAS and RXES experiments, though the derived valence is relatively higher than those obtained from the Yb  $3d$  HAXPES experiments. In the valence-band spectra, we found that the binding energy of the  $\text{Yb}^{3+}4f$  multiplet structures of  $\text{YbNi}_3\text{Al}_9$  is  $\sim 300$  meV higher than that of  $\text{YbNi}_3\text{Ga}_9$ . This suggests that

the energy difference between  $4f$ -hole level and  $E_F$  is small for  $\text{YbNi}_3\text{Ga}_9$  and large for  $\text{YbNi}_3\text{Al}_9$ . We also observed the energy shifts of the Ni  $2p$  and Ni  $3d$  states on going from  $X = \text{Al}$  to  $\text{Ga}$  by 300 meV toward the lower binding-energy side. These energy shifts can be explained by the  $E_F$  shift of the Ni-derived CB-DOS, which leads to the enhanced Ni  $3d$  DOS at  $E_F$  in  $\text{YbNi}_3\text{Ga}_9$ . Taking into account the  $4f$ -hole level close to  $E_F$ , the charge transfer from the Ni  $3d$  to Yb  $4f$  states easily takes place, which makes  $\text{YbNi}_3\text{Ga}_9$  valence fluctuating system.

### ACKNOWLEDGMENTS

The authors are grateful to Akio Kotani for fruitful discussion on the pressure and chemical substitution effects on the Yb  $4f$  states. We also thank Chikako Moriyoshi for valuable

comments on the crystal structures of  $\text{YbNi}_3\text{X}_9$ , Osamu Sakai and Shin Imada for the NCA calculation, and Hideki Iwasawa and Hirokazu Hayashi for the technical support for VUVPEs at HSRC. The synchrotron radiation experiments at SPring-8 were performed under the approval of NIMS Beamline Station (Proposal Nos. 2010B4801, 2011A4803, and 2011B4801) and Taiwan Beamline Station (Proposal Nos. 2011B4260 and 2012A4266). The VUVPEs experiments at HSRC is performed under the approval of HSRC (Proposal No. 11-A-12). This work was supported by Grants-in-Aid for Scientific Research on Innovative Areas “Heavy Electrons” (20102007, A01-23102712) from The Ministry of Education, Culture, Sports, Science, and Technology, Japan and (C: No. 23540411) from Japan Society for the Promotion of Science. One of authors (Y.U.) is grateful to Hayashi Memorial Foundation for Female Natural Scientist, the Chuo Mitsui Trust and Banking, Japan for the financial support.

\*utsumi-yuki@hiroshima-u.ac.jp

†jinjin@hiroshima-u.ac.jp

<sup>1</sup>C. M. Varma, *Rev. Mod. Phys.* **48**, 219 (1976).

<sup>2</sup>S. Nakatsuji, K. Kuga, Y. Machida, T. Tayama, T. Sakakibara, Y. Karaki, H. Ishimoto, E. Pearson, G. G. Lonzarich, H. Lee, L. Balicas, and Z. Fisk, *Nat. Phys.* **4**, 603 (2008).

<sup>3</sup>M. Okawa, M. Matsunami, K. Ishizaka, R. Eguchi, M. Taguchi, A. Chainani, Y. Takata, M. Yabashi, K. Tamasaku, Y. Nishino, T. Ishikawa, K. Kuga, N. Horie, S. Nakatsuji, and S. Shin, *Phys. Rev. Lett.* **104**, 247201 (2010).

<sup>4</sup>S. Ohara, T. Yamashita, Y. Mori, and I. Sakamoto, *J. Phys.: Conf. Ser.* **273**, 012048 (2011).

<sup>5</sup>T. Yamashita, R. Miyazaki, Y. Aoki, and S. Ohara, *J. Phys. Soc. Jpn.* **81**, 034705 (2012).

<sup>6</sup>R. E. Gladyshevskii, K. Genzual, H. D. Flack, and E. Parthé, *Acta Cryst. B* **49**, 468 (1993).

<sup>7</sup>Y. Lutsyshyn, Y. Tokaychuk, V. Davydov, and R. Gladyshevskii, *Chem. Met. Alloys* **1**, 303 (2008).

<sup>8</sup>S. Doniach, *Physica B & C* **91**, 231 (1977).

<sup>9</sup>S. Danzenbächer, Yu. Kucherenko, D. V. Vyalikh, M. Holder, C. Laubschat, A. N. Yaresko, C. Krellner, Z. Hossain, C. Geibel, X. J. Zhou, W. L. Yang, N. Mannella, Z. Hussain, Z.-X. Shen, M. Shi, L. Patthey, and S. L. Molodtsov, *Phys. Rev. B* **75**, 045109 (2007).

<sup>10</sup>J. L. Sarrao, C. D. Immer, Z. Fisk, C. H. Booth, E. Figueroa, J. M. Lawrence, R. Modler, A. L. Cornelius, M. F. Hundley, G. H. Kwei, J. D. Thompson, and F. Bridges, *Phys. Rev. B* **59**, 6855 (1999).

<sup>11</sup>J. M. Lawrence, P. S. Riseborough, C. H. Booth, J. L. Sarrao, J. D. Thompson, and R. Osborn, *Phys. Rev. B* **63**, 054427 (2001).

<sup>12</sup>S. Ueda, Y. Katsuya, M. Tanaka, H. Yoshikawa, Y. Yamashita, S. Ishimaru, Y. Matsushita, and K. Kobayashi, *AIP Conf. Proc.* **1234**, 403 (2010).

<sup>13</sup>K. Kobayashi, M. Yabashi, Y. Takata, T. Tokushima, S. Shin, K. Tamasaku, D. Miwa, T. Ishikawa, H. Nohira, T. Hattori, Y. Sugita, O. Nakatsuka, A. Sakai, and S. Zaima, *Appl. Phys. Lett.* **83**, 1005 (2003).

<sup>14</sup>I. Jarrige, H. Ishii, Y. Q. Cai, J.-P. Rueff, C. Bonnelle, T. Matsumura, and S. R. Shieh, *Phys. Rev. B* **72**, 075122 (2005).

<sup>15</sup>H. Yamaoka, I. Jarrige, N. Tsujii, N. Hiraoka, H. Ishii, and K.-D. Tsuei, *Phys. Rev. B* **80**, 035120 (2009).

<sup>16</sup>H. Yamaoka, H. Sugiyama, Y. Kubozono, A. Kotani, R. Nouchi, A. M. Vlaicu, H. Ohashi, T. Tochio, Y. Ito, and H. Yoshikawa, *Phys. Rev. B* **80**, 205403 (2009).

<sup>17</sup>H. Sato, K. Shimada, M. Arita, K. Hiraoka, K. Kojima, Y. Takeda, K. Yoshikawa, M. Sawadam, M. Nakatake, H. Namatame, M. Taniguchi, Y. Takata, E. Ikenaga, S. Shin, K. Kobayashi, K. Tamasaku, Y. Nishino, D. Miwa, M. Yabashim, and T. Ishikawa, *Phys. Rev. Lett.* **93**, 246404 (2004).

<sup>18</sup>J. Yamaguchi, A. Sekiyama, S. Imada, H. Fujiwara, M. Yano, T. Miyamachi, G. Funabashi, M. Obara, A. Higashiya, K. Tamasaku, M. Yabashi, T. Ishikawa, F. Iga, T. Takabatake, and S. Suga, *Phys. Rev. B* **79**, 125121 (2009).

<sup>19</sup>H. Sato, K. Yoshikawa, K. Hiraoka, M. Arita, K. Fujimoto, K. Kojima, T. Muro, Y. Saitoh, A. Sekiyama, S. Suga, and M. Taniguchi, *Phys. Rev. B* **69**, 165101 (2004).

<sup>20</sup>L. Moreschini, C. Dallera, J. J. Joyce, J. L. Sarrao, E. D. Bauer, V. Fritsch, S. Bobev, E. Carpena, S. Huotari, G. Vankó, G. Manaco, P. Lacovig, G. Panaccione, A. Fondacaro, G. Paolicelli, P. Torelli, and M. Grioni, *Phys. Rev. B* **75**, 035113 (2007).

<sup>21</sup>S. Suga, A. Sekiyama, S. Imada, A. Shigemoto, A. Yamasaki, M. Tsunekawa, C. Dallera, L. Braicovich, T.-L. Lee, O. Sakai, T. Ebihara, and Y. Ōnuki, *J. Phys. Soc. Jpn.* **74**, 2880 (2005).

<sup>22</sup>K. Yamamoto, H. Yamaoka, N. Tsujii, A. M. Vlaicu, H. Ohashi, S. Sakakura, T. Tochio, Y. Ito, A. Chainani, and S. Shin, *J. Phys. Soc. Jpn.* **76**, 124705 (2007).

<sup>23</sup>D. A. Shirley, *Phys. Rev. B* **5**, 4709 (1972).

<sup>24</sup>F. Reinert, R. Claessen, G. Nicolay, D. Ehm, S. Hüfner, W. P. Ellis, G.-H. Gweon, J. W. Allen, B. Kindler, and W. Assmus, *Phys. Rev. B* **58**, 12808 (1998).

<sup>25</sup>S. Tanuma, C. J. Powell, and D. R. Penn, *Surf. Interface Anal.* **21**, 165 (1994).

<sup>26</sup>C. Moriyoshi (private communication).

<sup>27</sup>J. J. Yeh and I. Lindau, *At. Data Nucl. Data Tables* **32**, 1 (1985).

<sup>28</sup>J. A. Leiro and M. H. Heinonen, *Surf. Sci.* **346**, 73 (1996).

<sup>29</sup>F. U. Hillebrecht, J. C. Fuggle, P. A. Bennett, Z. Zołnierak, and Ch. Freiburg, *Phys. Rev. B* **27**, 2179 (1982).



- <sup>30</sup>We carried out theoretical calculation based on SIAM with noncrossing approximation (NCA) and the NCA results reproduced the energy shift of  $\text{Yb}^{3+}$  multiplet structures toward the deeper binding-energy side with increasing the absolute value of  $\varepsilon_f$ .
- <sup>31</sup>T. Okane, S.-I. Fujimori, A. Ino, A. Fujimori, S. K. Dhar, C. Mitra, P. Manfrinetti, A. Palenzona, and O. Sakai, *Phys. Rev. B* **65**, 125102 (2002).
- <sup>32</sup>R. E. Gladyshevskii, K. Cenxual, and E. Parthé, *J. Alloys Compd.* **182**, 165 (1992).
- <sup>33</sup>K. Matsubayashi, T. Hirayama, T. Yamashita, S. Ohara, and Y. Uwatoko (in preparation).
- <sup>34</sup>A. V. Goltsev and M. M. Abd-Elmeguid, *J. Phys.: Condens. Matter* **17**, 5913 (2005).
- <sup>35</sup>E. R. Ylvisaker, J. Kunes, A. K. McMahan, and W. E. Pickett, *Phys. Rev. Lett.* **102**, 246401 (2009).
- <sup>36</sup>I. Felner and I. Nowik, *Phys. Rev. B* **33**, 617 (1986).
- <sup>37</sup>I. Felner, I. Nowik, D. Vaknin, Ulrike Potzel, J. Moser, G. M. Kalvius, G. Wortmann, G. Schmiester, G. Hilscher, E. Gratz, C. Schmitzer, N. Pillmayr, K. G. Prasad, H. de Waard, and H. Pinto, *Phys. Rev. B* **35**, 6956 (1987).
- <sup>38</sup>K. Kojima, *J. Magn. Magn. Mater.* **81**, 267 (1989).
- <sup>39</sup>C. Dallera, M. Grioni, A. Shukla, G. Vankó, J. L. Sarrao, J. P. Rueff, and D. L. Cox, *Phys. Rev. Lett.* **88**, 196403 (2002).
- <sup>40</sup>J. M. Lawrence, S. M. Shapiro, J. L. Sarrao, and Z. Fisk, *Phys. Rev. B* **55**, 14467 (1997).
- <sup>41</sup>Y. Utsumi, H. Sato, H. Kurihara, H. Maso, K. Hiraoka, K. Kojima, K. Tobimatsu, T. Ohkuchi, S.-I. Fujimori, Y. Takeda, Y. Saitoh, K. Mimura, S. Ueda, Y. Yamashita, H. Yoshikawa, K. Kobayashi, T. Oguchi, K. Shimada, H. Namatame, and M. Taniguchi, *Phys. Rev. B* **84**, 115143 (2011).